Molecular Recognition of Oligosaccharide Epitopes by a Monoclonal Fab Specific for *Shigella flexneri* Y Lipopolysaccharide: X-ray Structures and Thermodynamics[†,‡]

Nand K. Vyas,[§] Meenakshi N. Vyas,[§] Mary C. Chervenak,[⊥] Margaret A. Johnson,[∥] B. Mario Pinto,[∥] David R. Bundle,[⊥] and Florante A. Quiocho*[,§]

Verna and Marrs Mclean Department of Biochemistry and Molecular Biology and Howard Hughes Medical Institute, Baylor College of Medicine, Houston, Texas 77030, Departments of Chemistry and of Molecular Biology and Biochemistry, Simon Fraser University, Burnaby, British Columbia, Canada V5A 1S6, and Department of Chemistry, University of Alberta, Edmonton, Alberta, Canada T6G 2G2

Received May 16, 2002; Revised Manuscript Received August 26, 2002

ABSTRACT: The antigenic recognition of *Shigella flexneri O*-polysaccharide, which consists of a repeating unit ABCD [→2)-α-L-Rha*p*-(1→2)-α-L-Rha*p*-(1→3)-α-L-Rha*p*-(1→3)-*β*-D-Glc*p*NAc-(1→], by the monoclonal antibody SYA/J6 (IgG3, *κ*) has been investigated by crystallographic analysis of the Fab domain and its two complexes with two antigen segments (a pentasaccharide Rha A−Rha B−Rha C−GlcNAc D−Rha A′ and a modified trisaccharide Rha B−Rha C*−GlcNAc D in which Rha C* is missing a C2−OH group). These complex structures, the first for a Fab specific for a periodic linear heteropolysaccharide, reveal a binding site groove (between the V_H and V_L domains) that makes polar and nonpolar contacts with all the sugar residues of the pentasaccharide. Both main-chain and side-chain atoms of the Fab are used in ligand binding. The charged side chain of Glu H50 of CDR H2 forms crucial hydrogen bonds to GlcNAc of the oligosaccharides. The modified trisaccharide is more buried and fits more snugly than the pentasaccharide. It also makes as many contacts (∼75) with the Fab as the pentasaccharide, including the same number of hydrogen bonds (eight, with four being identical). It is further engaged in more hydrophobic interactions than the pentasaccharide. These three features favorable to trisaccharide binding are consistent with the observation of a tighter complex with the trisaccharide than the pentasaccharide. Thermodynamic data demonstrate that the native tri- to pentasaccharides have free energies of binding in the range of 6.8−7.4 kcal mol^{-1}, and all but one of the hydrogen bonds to individual hydroxyl groups provide no more than ∼0.7 kcal mol^{-1}. They further indicate that hydrophobic interactions make significant contributions to binding and, as the native epitope becomes larger across the tri-, tetra-, pentasaccharide series, entropy contributions to the free energy become dominant.

Polysaccharide and oligosaccharide antigens in the form of synthetic conjugate vaccines are the subject of intense research interest and practical applications to combat infectious diseases (*1*) and as auxiliary treatments in certain cancer therapies (*2*). The design of conjugate vaccines should benefit from detailed structural studies of oligosaccharide−antibody complexes, but before this objective can be realized, it is essential to expand the limited structural database for such complexes. To date, the crystal structures of only three bacterial Fab−carbohydrate complexes have been determined: the mAb Se155-4 specific for a *Salmonella* serotype-B *O*-Ag (*3*), an anti-cholera murine mAb S-20-4 specific for the lipopolysaccharide Ag of the Ogawa serotype (*4*), and SYA/J6 reported here. A fourth complex of a tumor-specific Fab (*5*) with the Lewis Y epitope completes the group of structures for which electron density defines the interactions of the bound carbohydrate epitope. Several structures of carbohydrate-specific Fab are known that fail to provide this crucial data (*6*−*9*). An expansion of the very small sample set of Fab−oligosaccharide complexes is required to confirm the emerging trend of epitope size, its location within a polysaccharide antigen, and the implications of such structural detail for the new generation of conjugate vaccines (*10*).

The lipopolysaccharides (LPS)[1] are a major structural component of the cell surface of Gram-negative bacteria; an estimate of 2.5×10^6 molecules per cell suggests that

[†] This work was supported by grants from NIH (AI 40061 to N.K.V., and GM 21371 to F.A.Q.) and the Welch Foundation (to F.A.Q), the Natural Sciences and Engineering Research Council of Canada (NSERC) (to D.R.B. and B.M.P), and an NSERC postgraduate fellowship (to M.A.J.). F.A.Q. is Investigator in the Howard Hughes Medical Institute.

[‡] The atomic coordinates have been deposited in the Protein Data Bank (accession numbers 1M71, 1M7D, and 1M7I).

* To whom correspondence may be addressed. Telephone: (713) 798-6565; Fax: (713) 798-8516; E-mail: faq@bcm.tmc.edu

[§] Baylor College of Medicine.

[∥] Simon Fraser University.

[⊥] University of Alberta.

[1] Abbreviations: Ab, antibody; ABCDA′, Rha A−Rha B−Rha C−GlcNAc D−Rha A′; BC*D, Rha B−Rha C*−GlcNAc D; CDR, complementarity-determining region; Fab, fragment with antigen binding; GlcNAc, *N*-acetylglucosamine; H1, heavy chain CDR1; IgG3, *κ*, immunoglobulin G, heavy chain class 3, light chain class *κ*; L1, light chain CDR 1; LPS, lipopolysaccharide; mAb, monoclonal antibody; Rha, rhamnose; V_H, variable heavy chain; V_L, variable light chain.

10.1021/bi0261387 CCC: $22.00
Published on Web 10/26/2002

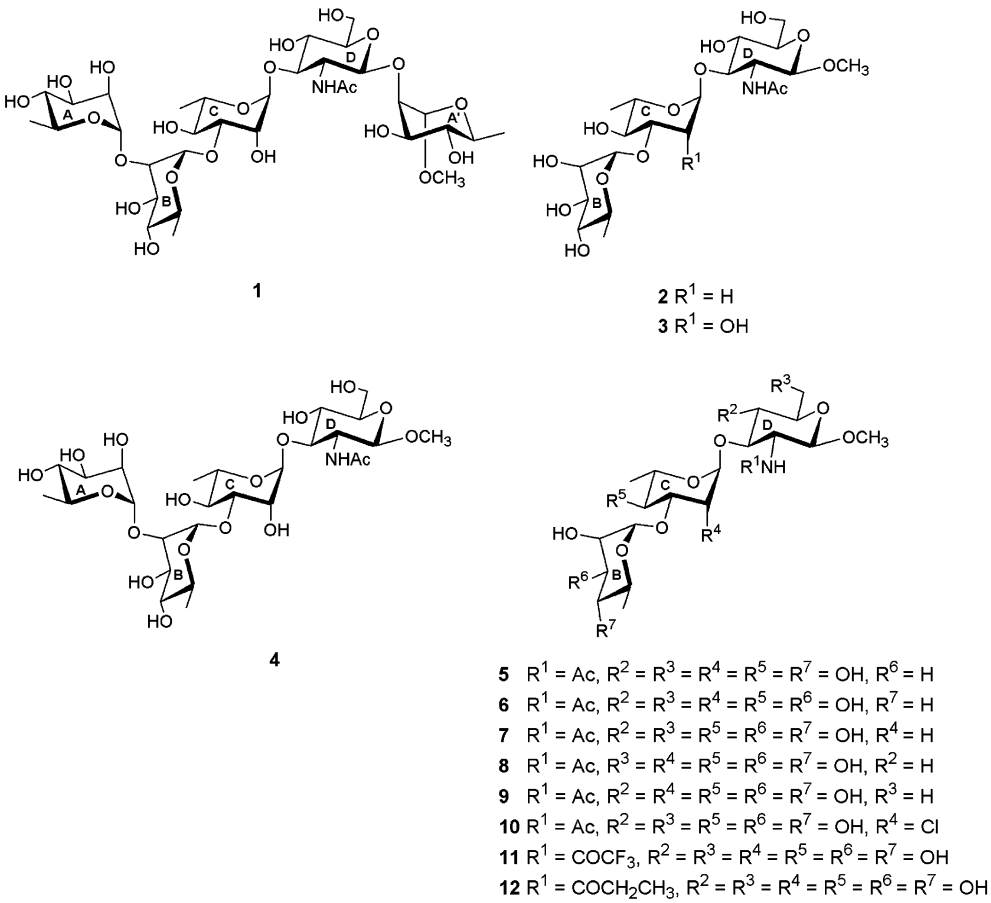

FIGURE 1: Schematic diagram of the synthetic oligosaccharides corresponding to the *O*-polysaccharide of *S. flexneri* Y used in this study. The pentasaccharide ABCDA′ (**1**) represents a repeating unit ABCD [→2)-α-L-Rha*p*-(1→2)-α-L-Rha*p*-(1→3)-α-L-Rha*p*-(1→3)-*β*-D-Glc*p*NAc-(1→] of the antigen and the first sugar (A′) of the next repeating unit. The modified trisaccharide (BC*D) (**2**) is an analogue in which the C residue is 2-deoxy-Rha. Compounds **3** and **4** are the native trisaccharide and tetrasaccharide, respectively. The remaining compounds contain further modifications intended to probe their effects on the thermodynamics of binding (Table 6).

they occupy about 45% of the outer membrane surface (*11*). The host humoral response to *Shigella* is dominated by LPS-specific antibodies, and although the precise mechanism of serotype specific immunity is not well understood for this bacterium, developers of *Shigella* vaccines envision the LPS *O*-antigen as an essential component (*12*, *13*). Whereas it is known that to function as protective immunogens, glycoconjugates must contain oligosaccharides ranging in length from 2 to 13 repeating units (*10*, *14*), there is scant information about the molecular details of the antibody−antigen complex that presumably initiates the events leading to immunity (*13*).

We report here the determination of three X-ray structures of a Fab fragment of a murine monoclonal antibody, SYA/J6 (IgG3, *κ*) (*15*), generated in response to immunization with bacterial cells of *Shigella flexneri* variant Y (*15*, *16*). The antibody binds an optimal trisaccharide epitope, a residue sequence BCD of the ABCD [→2)-α-L-Rha-(1→2)-α-L-Rha-(1→3)-α-L-Rha-(1→3)-*β*-D-GlcNAc-(1→] repeating unit of the *O*-polysaccharide of the *S. flexneri* variant Y LPS (Figure 1) (*17*). Structures are reported for the native Fab and two complexes with the natural pentasaccharide **1** (ABCDA′) (Figure 1) and a trisaccharide **2** (BC*D) epitope with a synthetic 2-deoxy-L-Rha at the C sugar (Figure 1). These structures are the first to be determined for a Fab specific for a periodic linear heteropolysaccharide in the presence and absence of bound ligands. They further provide an indication of the fidelity of binding site topography inferred from binding site mapping, since the SYA/J6 antibody site was the subject of intense molecular modeling work prior to the completion of the crystal structure determination (*17*). This is especially relevant to the monodeoxy trisaccharide analogue BC*D, which has about 17- and 7-fold enhanced affinity relative to the native trisaccharide sequence BCD **3** and the ABCDA′ pentasaccharide, respectively.

MATERIALS AND METHODS

Crystals and Diffraction Data Collection. The crystallization of the Fab of antibody SYA/J6 and its complexes with BC*D and ABCDA′ has been described previously (*15*). All three crystal forms of Fab belong to the space group $P4_32_12$ or $P4_12_12$ with cell dimensions as shown in Table 1. Data to medium- and high-resolution range were obtained at beamline BL6A2 at the Photon Factory synchrotron facility (Tsukuba, Japan). The diffraction data were collected by the Weissenberg method using Fuji imaging plates (*18*). The crystal to detector distance was 430 mm and X-rays of wavelength 1.0 Å were used. The Weissenberg camera chamber was filled with helium at 6 °C. The raw data from each imaging plate were indexed and reduced with the WEIS software (*19*), and the reduced data from all the imaging plates were merged in the PROTEIN software package (W. Steigemann). The statistics for the data collection are shown in Table 1.

Table 1: Crystal and Diffraction Data and Refinement Statistics

item	Fab	Fab−BC*D complex	Fab−ABCDA′ complex
space group	$P4_32_12$	$P4_32_12$	$P4_32_12$
unit cell parameters (Å)			
$a = b$	70.7	71.0	70.5
c	202.4	198.0	203.1
resolution (Å)	2.8	2.3	2.5
total reflections measured	108 812	112 922	108 148
no. of unique reflections ($I > 1.5\ \sigma I$)	10 392	17 923	14 375
completeness % (outer shell)[a]	77.9 (59.9)	76.7 (51.3)	79.6 (55.2)
R-merge	11.6	7.3	9.7
no. of residues or solvent			
L-chain	215	215	215
H-chain	220	220	220
solvent	62	121	171
R-cryst (outer shell)[a]	0.223 (0.375)	0.214 (0.285)	0.207 (0.389)
R-free[b] (outer shell)[a]	0.292 (0.410)	0.278 (0.327)	0.279 (0.411)
rms deviation			
bond distance (Å)	0.007	0.007	0.007
bond angle (deg)	1.4	1.4	1.4
Ramachandran plot statistics (%) (excluding Gly and Pro)			
most favored regions	76.1	87.9	86.3
additionally favored regions	22.3	11.3	12.9
generally allowed regions	1.3	0.5	0.5
disallowed regions	0.3	0.3	0.3

[a] Values in the parentheses are for highest resolution shells: 2.97−2.80 Å for Fab, 2.44−2.30 Å for the complex with BC*D, and 2.66−2.50 Å with bound ABCDA′. [b] Calculated using a random 5% of the reflection data omitted in the refinement.

Structure Determination and Refinement. The crystal structure of the SYA/J6 Fab−ABCDA′ complex was successfully determined by the molecular replacement method in space group $P4_32_12$ using the MERLOT package of computer programs (P. Fitzgerald, Merck Co.) and a 3.5 Å diffraction data set. The McPC603 Fab coordinates (accession number 1MCP (*20*)) were used as the search molecule. The center of mass of the search molecule was placed at the origin of an orthogonal cell. Rotation search yielded values of $\alpha = 62.36°$, $\beta = 83.14°$, $\gamma = 281.44°$, and the translation search gave values of tx = 0.260, ty = 0.450, tz = 0.160.

Calculation of close contact distances between $C_\alpha - C_\alpha$ atoms of symmetry-related molecules using the initial model of the SYA/J6 Fab in $P4_32_12$ indicated only one short intermolecular contact of less than 5 Å. The initial model of the SYA/J6 Fab−ABCDA′ complex was further refined by the rigid-body refinement method in the CNS package of programs (*21*). The initial refinement using the 8.0−4.5 Å resolution data reduced the *R*-factor to 0.47, and when individual domains were refined separately as rigid bodies, the *R*-factor further decreased slightly to 0.43. Following a few cycles of slow annealing refinement using 6.0−3.5 Å resolution data, significant improvement in the quality of electron density maps was seen, and the *R*-factor dropped to 0.30. An electron density map ($2|F_o| - |F_c|$) that was calculated at this juncture using calculated phases from the model revealed several details consistent with a Fab structure, including most impressively the presence of a bound antigen in the combining site of V_L and V_H domains.

Because of the close similarity of the crystals of the unliganded Fab and the complex with BC*D with that of the Fab−ABCDA′ complex (*15*), their structures were determined in a straightforward manner by direct phasing with the structure of the complex with ABCDA′. Because the crystal of the Fab−BC*D complex diffracted better than the native Fab and Fab−ABCDA′ complex crystals, it was the first structure to be refined (Table 1). The refinement was carried out by CNS using its slow annealing protocol (*21*), and manual fitting of the Fab model into the electron density maps was done after each refinement cycle. The amino acid sequence following the Kabat and Wu convention of the SYA/J6 Fab (D. C. Watson, D. Bilous, S.-J. Deng, M. A. J. Gidney, D. R. Bundle, and N. M. Young, unpublished) was used in fitting to the electron density maps. For molecular model building of the ligand-free Fab and Fab−carbohydrate complexes into the electron density maps, we used the molecular graphics program CHAIN (*22*).

For all the three structures, the amino acids of the light and heavy chains of SYA/J6 Fab and the bound carbohydrate for the liganded Fab could be fitted by iterative cycles of refining and manual fitting in the ($2|F_o| - |F_c|$) and the ($|F_o| - |F_c|$) electron density maps. The electron density maps were calculated using the refined phases and observed structure factors of the Fab and the liganded Fab structures.

For further refinement, the stereochemistry of all three Fab structures was tightly restrained. Moreover, the occupancy of the bound trisaccharide and tetrasaccharide refined to 0.81 and 0.65, respectively, which made their *B*-values comparable to those of surrounding residues. The statistics for the refinements are shown in Table 1. With few exceptions, in all three structures, the main-chain conformational angles (ϕ,ψ) of all residues conform well within the minimum energy regions of the Ramachandran plot calculated by PROCHECK (*23*). The estimated root-mean-square errors in coordinates of the three structures based on the Luzzati plots (*24*) range between 0.3 and 0.4 Å. In all three structures, the segment of residues H128−H135 shows no interpretable density, which is typically observed in Fab structures.

Modeling of Antibody−Polysaccharide Interaction. The Fab−ABCDA′ complex structure served as a starting point for building a model of the *O*-polysaccharide that consists of a linear left-handed helical chain of three repeating units

of the tetrasaccharide ABCD (A″B″C″D″ABCDA′B′C′D′) (*25*, *26*). This was accomplished by extending both ends of the ABCDA′ bound in the structure. The initial glycosidic torsion angles of A″B″C″D″, ABCD, and A′B′C′D′ were identical to those of the ABCD segment of the bound pentasaccharide. However, to achieve a better fit and avoid steric clashes, the torsion angle of the D−A′ linkage was adjusted slightly close to the value for a left-handed helical polysaccharide (*25*). No changes were required in the structure of the Fab to accommodate the modeled *O*-polysaccharide in the combining site. The model of Fab−polysaccharide was not energy minimized, although no steric clash was observed between the Fab and model. The CHAIN program (*22*) was used for the modeling of the *O*-polysaccharide complex and for measuring the intermolecular contacts.

Titration Microcalorimetry. Antibody was purified from ascites fluid by centrifugation (30 min, 64000*g*) to pellet cells and fatty tissue. After filtration first through a Millex AP 20 prefilter (Millipore) and then through a Millex-GV 0.22 μm low-binding sterilization filter (Millipore), the filtrate was loaded onto a Sepharose Protein A (Pharmacia Biotech) column equilibrated with running buffer (50 mM Tris, 150 mM NaCl, 0.02% NaN_3, adjusted to pH 8.0). The column was washed with running buffer until serum proteins were eluted (absorbance at 280 nm below 0.1). Antibody was then eluted with citrate buffer (100 mM citric acid, 150 mM NaCl, 0.02% NaN_3, adjusted to pH 3.0). Fractions with an absorbance greater than 0.1 were collected, pooled, and dialyzed (24 h) against the initial Tris buffer. Dialyzed antibody was concentrated and equilibrated against the buffer used for calorimetry in CentriPrep units (Amicon). Antibody concentration was determined spectrophotometrically, using a calculated extinction coefficient of 1.53 mg^{-1} mL (*27*).

Dry saccharide samples were prepared as a 2 mM stock solution and assayed for carbohydrate concentration as previously described (*28*).

Calorimetric measurements were made using the Microcal MCS titration microcalorimeter (*28*, *29*). Purified antibody (IgG, 20 to 100 μM) was placed in the cell and titrated with ligand. In all cases, the value *C*, defined as the product of the binding constant *K* and the concentration of binding sites, was in the range of 1−500, and ligand concentrations were such that the final ligand concentration was at least $10K_D$. Titrations of the antibody and data processing were carried out as previously described (*28*, *30*). The measurements were evaluated by the ORIGIN software package (MicroCal Inc., Northhampton, MA) and data were processed using a single binding site model that assumes no cooperativity between sites (Table 6). Standard deviation refers to the mean value of two experiments performed under identical conditions.

RESULTS AND DISCUSSION

SYA/J6 Fab Structure. The refined structures of the SYA/J6 Fabs with and without bound oligosaccharides have *R*-factors ranging from 20.7 to 22.3%, *R*-free from 27.8 to 29.2%, and reasonably good geometry (Table 1).

The three structures display the common immunoglobulin fold and show no large conformational differences (Figure 2A). Least squares superpositioning of the Cα atoms of the three structures yields rms differences in the range of 0.2−0.9 Å. Similar values have been obtained in comparing other Fab structures with or without bound antigens (*31*). When all non-hydrogen atoms of CDRs are superimposed, the rms differences in atomic positions range from 0.8 to 1.9 Å.

The Fab is composed of a heavy and light chain in which the variable domains associate along a pseudo-2-fold symmetry (Figure 2A). The conformation of the complementarity-determining regions (CDRs) (except CDR H3) fall into the canonical structure classes (*32*−*34*). The base of the CDR H3 loop shows the TB (torso bulged) structure (*35*). The rest of this loop is highly variable and no canonical structures are known for it. Accordingly, its conformation in the SYA/J6 Fab does not resemble those of other loops in the database. The structures of CDRs L1 and L2 are of the classes 4/16A and 1/7A, respectively (*34*). CDRs H1 and H2 are of the classes 1/10A and 4/12B. CDR L3 contains only eight residues, one residue shorter than the usual; residue L96 is deleted, while the conserved Pro residue is at position L95. The same deletion occurs in the anti-lysozyme antibody HyHEL-5 and was estimated to occur in 1% of mouse antibody sequences and 2% of human antibody sequences (*33*). CDR L3 adopts the unusual canonical structure 6, observed in only three other antibody structures. The catalytic antibody 17E8 (*36*) and the anti-protein antibody CRIS-1 (*37*) lack a proline residue in L3 and this was proposed as a key determinant of this canonical structure (*37*). On the basis of sequence, the SYA/J6 L3 would have been classified as class 3, similar to HyHEL-5. However, the top residues of the loop adopt a different conformation from those in HyHEL-5, and the loop is different by the criteria of Martin and Thornton (*34*). In contrast, the loop α-carbons superimpose with rmsd = 0.5 Å on those of the loop in antibody 17E8, and the placement of side chains is very similar. The Pro residue at L95 takes the place of Arg L96 in 17E8. Previously, it was proposed that the Pro residue constrained the L3 loop in canonical structure 1/2, 3, or 4, depending on its length (9, 8, or 10 residues), while canonical structures 5 and 6 were determined by the absence of Pro (*37*). The SYA/J6 structure and that of the antibody MN14C11.6 (*38*) show that this is not the case: canonical structure 6 may be adopted by eight-residue loops containing Pro.

In the center of the antigen-binding site, three CDRs (L3, H3, and L1) are linked in a three-way network of hydrogen bonds by way of Thr L91. The OG1 of the Thr residue donates a hydrogen bond to the carbonyl oxygen of Gly H99 and accepts a hydrogen bond from the side chain of His L34. It is further involved in a hydrogen bond with the C2 hydroxyl group of the Rha C residue of the bound pentasaccharide. Moreover, the Thr peptide NH is a donor to the CO group of Tyr L32, and the peptide CO is an acceptor from the NH moiety of the acetamido group of the GlcNAc D unit of both bound oligosaccharides. A water molecule in the unliganded structure occupies the position of the NH moiety.

As the H3 makes the greatest number of interactions with the bound sugars, it plays a major role in conferring antigen specificity. This CDR has well-defined density in all three structures. The presence of three glycine residues (H95, H96 and H99) in the H3 loop, which contributes to the antigen specificity of the Fab, is consistent with the general observation of the high frequency of this type of residue in other Fab structures (*31*).

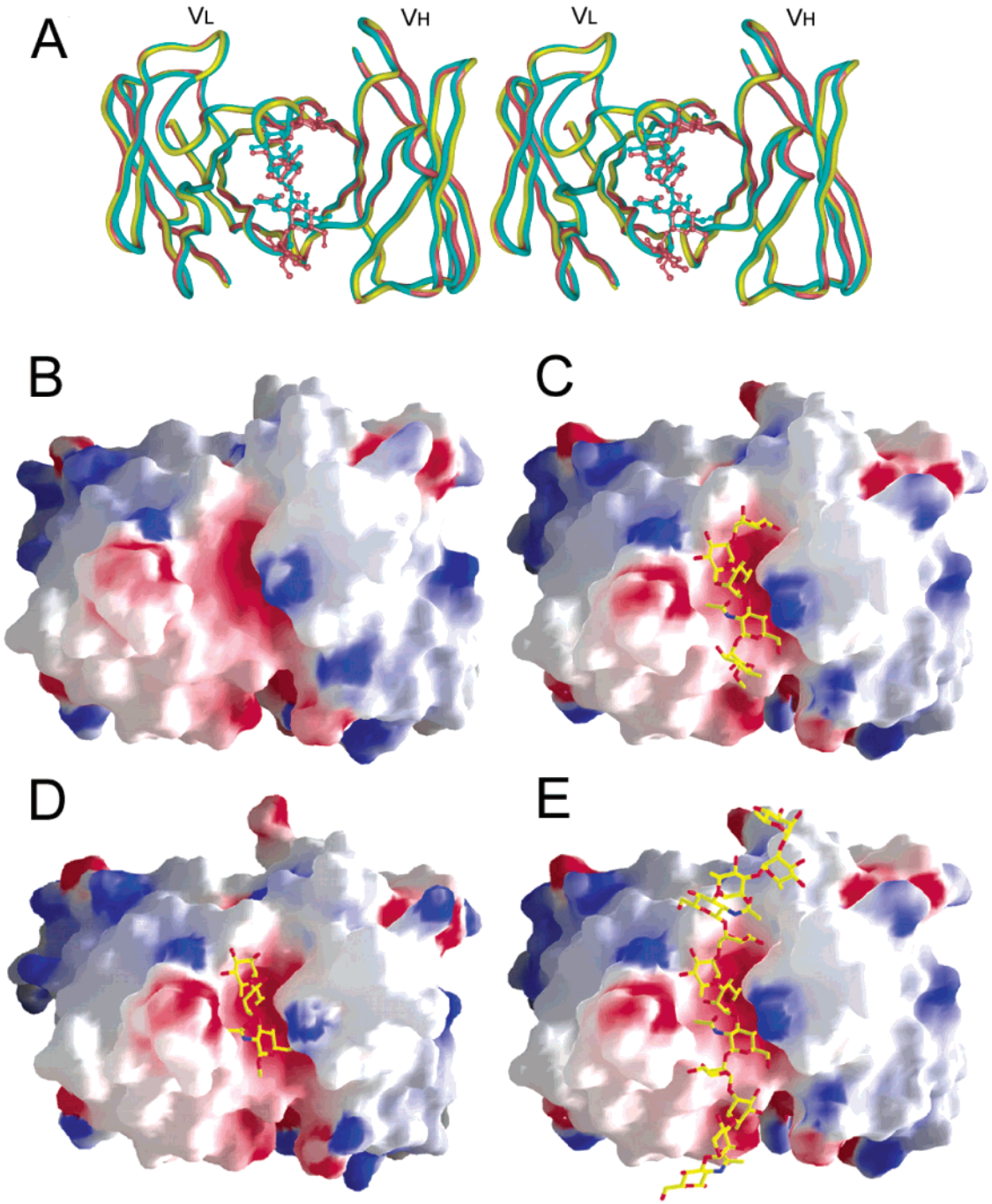

FIGURE 2: Structures of a Fab fragment of the murine monoclonal antibody SYA/J6 specific for *S. flexneri* Y lipopolysaccharide. (A) Stereoview of the superimposed backbone traces of the carbohydrate-free Fab (yellow) and its complexes with ABCDA′ (mauve) and BC*D (blue) using MIDAS molecular graphics package (*39*). The variable light and heavy chains are labeled V_L and V_H, respectively. GRASP (*40*) electrostatic surface potential (−10 kT, red; neutral, white; +10 kT, blue) of the Fab: (B) unliganded, (C) with bound pentasaccharide **1**, (D) with bound trisaccharide **2**, and (E) with modeled *O*-polysaccharide. All figures are in the same orientation. The bottom sugar residue of the oligosaccharides is the reducing end.

The Combining Site with Bound Oligosaccharides. The most interesting aspect of the structural analysis is the determination of the binding modes of two oligosaccharide segments of the cell surface antigen, a natural pentasaccharide α-L-Rha*p*-(1→2)-α-L-Rha*p*-(1→3)-α-L-Rha*p*-(1→3)-*β*-D-Glc*p*-NAc-(1→2)-α-L-Rha*p* (ABCDA′) (**1**) (Figure 1) and a modified trisaccharide (BC*D) (**2**) missing the C2−OH of Rha C (Figure 1).

Each bound oligosaccharide displays for the most part clearly interpretable electron density (Figures 3A and B). In fitting the density of the carbohydrates, we initially used the models of the natural trisaccharide and pentasaccharide derived from combined NMR analysis and theoretical calculations (*25*). The conformations of these models differ to some degree from those of the bound oligosaccharides in the refined structures (discussed below).

The ABCDA′ and the BC*D oligosaccharides show very good shape complementarity with the binding site (Figure 2A,C,D). The antigen-combining site is a groove about 25 Å long and at the center about 10 Å deep and 12 Å wide, and it runs parallel to the interface of the V_L and V_H domains. The surface of the groove is lined by all six CDRs, namely

Table 2: Accessibility of the Free and Fab-Bound Pentasaccharide (**1**) and Modified Trisaccharide (**2**)

	solvent accessible surface area (ASA)					
	ABCDA′ (**1**)			BC*D (**2**)		
sugar residues	free (Å^2)	bound (Å^2)	ratio[a] (%)	free (Å^2)	bound (Å^2)	ratio[a] (%)
Rha A	208	88	42			
Rha B	154	65	42	215	42	20
Rha C (C*)	154	3	0	151	0	0
GlcNAc D	218	21	10	327	38	12
Rha A′	249	161	65			
overall	983	338	34	693	80	12

[a] The ratio (in %) of the solvent-accessible surface area of the Fab-bound and unbound sugars, i.e., (bound/free) × 100.

L1 (L24−L34), L2 (L50−L56), and L3 (L89−L97) and H1 (H31−H35), H2 (H50−H65), and H3 (H95−H102). Although both polar and nonpolar residues line the groove, significantly more polar residues with mostly negatively charged carboxylate side chains are present (Figure 2B−D).

The bound ABCDA′ is more exposed to the bulk solvent than the bound BC*D; about 66% and 88% of the free accessible surface of the ABCDA′ and BC*D, respectively, are buried (Table 2). In both complexes, the middle Rha C or C* residue, which occupies the deepest center of the groove (Figure 2B,C), is completely inaccessible to bulk solvent, whereas the flanking residues Rha B and GlcNAc D are exposed to bulk solvent to varying extent (Table 2). The terminal residues, A and A′, are near the periphery of the site and considerably exposed (Table 2). The accessible surface area, calculated using a water molecule with a 1.4 Å radius as a probe (*41*), for each sugar residue follows the order A′ > A > B > D > C for the bound pentasaccharide and B > D > C* for the trisaccharide.

Mode of Binding of the Pentasaccharide. The bound ABCDA′ makes a total of 74 contacts (≤4 Å distance) with only the CDRs of the Fab (Figure 3C and Table 3). With the exception of L2, all CDR segments contact the sugar residues. Whereas recognition of Rha A at the nonreducing end is achieved by interactions solely with the V_H residues, Rha A′ at the reducing end is accomplished by contacts exclusively with V_L residues. In contrast, both light and heavy chains participate in binding of the middle sugars Rha B, Rha C, and GlcNAc D. The C6 of Rha C and one face of the ring interact with hydrophobic residues (Met H100A, Gly H99) as well as Thr L91 on the bottom of the site. The flanking residues Rha B and GlcNAc D form specific hydrogen bonds with key residues in the site (see below). The D sugar, with its N-acetamido group, is engaged in the largest number of contacts, 4 times more with the light chain (13 contacts) than with the heavy chain (3 contacts).

Of the 74 contacts in the Fab−ABCDA′ complex, eight are hydrogen bonds (<3.4 Å distances) that are made with an equal number of residues from the heavy and light chain CDRs (Figure 3C and Table 3). Two water molecules are also hydrogen bonded to the carbohydrate. Of the eight direct hydrogen bonds, three involve main chain carbonyl oxygen acceptor atoms and five involve side chain atoms. With the exception of one charged−neutral hydrogen bond involving the C4−OH group of GlcNAc D, all the hydrogen bonds are of the neutral−neutral type. Rha B is somewhat solvent-exposed; its C6 makes no contact with the site, but its C3− and C4−OH groups form hydrogen bonds to Ala H97 O and Tyr L32 OH, respectively. As the C2−OH group of Rha C is a donor to the backbone carbonyl oxygen of Gly H99 and an acceptor from the OG1 group of Thr L91, it is engaged in a stable cooperative hydrogen-bonding interaction. Thr L91 OG1 further donates a hydrogen bond to the carbonyl oxygen of Gly H99 (Figure 3C).

Essential hydrogen bonds are formed by GlcNAc D, including those between 2-NH and Thr L91 O and C4−OH and Glu H50 OE1, which is in turn salt linked with Arg H52. Interestingly, a cation−π interaction (*42*) is formed between Arg H52 and Trp H33. A rarity among oligosaccharides bound to proteins is the involvement of both glycosidic bond (O1) and ring (O5) oxygens of GlcNAc D in hydrogen bonding a water molecule.

*Mode of Binding of BC*D and Comparison with the Bound ABCDA′.* The bound BC*D makes 75 contacts (≤4.0 Å) with the Fab, almost equal to those made with the bound ABCDA′. This is indicative of a better fit of BC*D to the binding site groove. Both the light and heavy chains interact with the three sugar residues. Relative to that of the ABCDA′, the binding of BC*D causes some adjustments of both sugar and Fab side chains in order to achieve better complementarity. These adjustments revolve mainly around Rha C* and GlcNAc D (discussed below).

BC*D is engaged in a total of eight hydrogen bonds with six Fab residues (Ala H97, Tyr L32, Gly H96, Thr L91, Glu H50, and Arg H52) (Figure 3D and Table 4). It also makes one hydrogen bond with a water molecule that is in turn hydrogen bonded to Arg H52. Both BC*D and ABCDA′ are engaged in the same number of hydrogen bonds, but only four are identical. Five of the eight hydrogen bonds are formed with GlcNAc D, of which four are the charged−neutral type. Although the Rha C* is completely buried (Table 2), it makes fewer interactions (both hydrogen bonds and van der Waals contacts combined) than GlcNAc D, which is partially exposed. Since Rha C of BC*D is missing the C2−OH, it lacks the two hydrogen bonds to this OH group in the bound ABCDA′ with Thr L91 OG1 and Gly H99 O. Nevertheless, the hydrogen bond between Thr L91 OG1 and Gly H99 O formed in the complex with ABCDA′ (Figure 3C) is maintained with BC*D (Figure 3D), thereby leaving no unpaired polar groups in the buried environment.

Compared to the involvement of only two hydrogen bonds with the GlcNAc D of ABCDA′, six hydrogen bonds are formed with the same sugar residue of BC*D, five directly with the protein and one indirectly via a water molecule. Five of these hydrogen bonds form a network involving C4−OH; C6−OH; acetamido groups of GlcNAc; residues Arg H52, Glu H50, and Thr L91; and a water molecule. The network is facilitated by a gauche−gauche conformation of the C6−OH group (Figure 3D). The gauche−trans conformation in the bound ABCDA′ precludes a hydrogen-bond network (Figure 3C). Glu H50 plays a central role in the formation of the network by accepting two bifurcated hydrogen bonds from C6−OH and one hydrogen bond from C4−OH and by keeping Arg H52 in place through one hydrogen bond. By further accepting a hydrogen bond from NH1 of Arg H52, the C6−OH is engaged in a stable cooperative hydrogen bond. The network is completed by

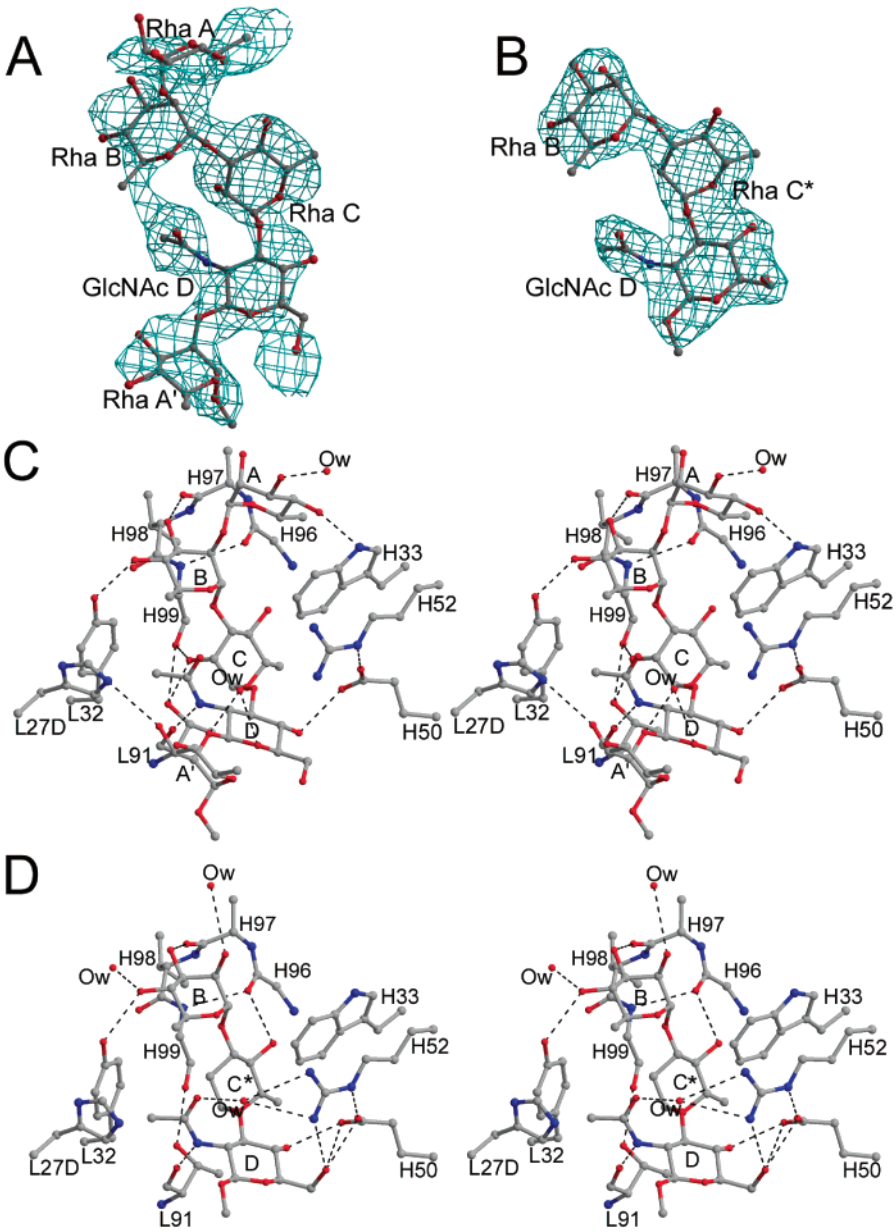

FIGURE 3: Oligosaccharides bound to the Fab structures. (A) The 2.8 Å resolution difference electron density of the bound ABCDA′ contoured at the 2σ level. (B) The 2.3 Å difference electron density of the bound BC*D contoured at the 2σ level. (C and D) Stereoviews of the hydrogen bonds (<3.4 Å) between the Fab and ABCDA′ and BC*D, respectively. See also Tables 3 and 4. Figure 3 and 4 are drawn using MOLSCRIPT software (*43*).

the formation of the water-mediated hydrogen bond between the acetamido carbonyl oxygen (O7) and Arg H52. This water-mediated hydrogen bond is missing in the complex with ABCDA′, although a water is present in a location near that in the BC*D complex (Figure 2C). However, the water molecule is hydrogen bonded to the oxygens of the D sugar ring oxygen and the glycosidic bond. We have no clear explanation for why the network of hydrogen bonds is absent in the binding of ABCDA′ (Figure 3C), especially since the gauche−trans conformation of the C6−OH of the GlcNAc is also energetically favorable.

The complex with BC*D, with an equilibrium association constant or K_A of 1.7×10^6 M^{-1} (see also Table 6 below), is about 7- and 17-fold tighter than those with the ABCDA′ and the natural trisaccharide **3** (BCD) epitopes (*16*). The structural data offer understanding of the reasons for the differences in affinities, with hydrophobic interactions clearly favoring the complex with BC*D.

There are three major pieces of evidence for more favorable nonpolar interactions with BC*D than with ABCDA′. First, the C8 methyl moiety of the exocyclic acetamido group of the GlcNAc D of the BC*D fits more snugly in the hydrophobic pocket formed by Tyr L32, His L27D, and Rha C (Figure 4B) than that of the bound ABCDA′ (Figure 4A). The better fit of the C8 methyl group is promoted by changes of three torsion angles of the bound BC*D relative to those of the bound ABCDA′. (i) The torsion angle (χ2) of His L27D changes by 16°. The hydrogen-bonding interaction between His L27D NE2 and C3−OH of Rha A′ of the pentasaccharide (Figure 3C) is largely responsible for fixing the geometry of the His residue and thus preventing similar favorable placement of the C8 methyl

Table 3: Stabilizing Interactions for the ABCDA′ (**1**) Binding to Fab

sugar residue		Fab residue	distance (Å)
		H-bonds (d < 3.4 Å)	
Rha A	(4-OH)	CDR-H1: Trp H33 (NE1)	2.70
Rha B	(3-OH)	H3: Ala H97 (O)	3.02
	(4-OH)	L1: Tyr L32 (OH)	2.52
Rha C	(2-OH)	L3: Thr L91 (OG1)	2.92
	(2-OH)	H3: Gly H99 (O)	3.15
GlcNAc D	(2-NH)	L3: Thr L91 (O)	2.68
	(4-OH)	H2: Glu H50 (OE1)	2.81
Rha A′	(3-OH)	L1: His L27D (NE2)	3.21
		H-bonds via H_2O links (d < 3.4 Å)	
		none	
		H-bonds with H_2O (d <3.4 Å)	
Rha A (3-OH)		w1	2.42
GlcNAc D (O5)		w2	3.11
Rha A′ (1-O)		w2	2.60
		van der Waals contacts (d < 4.0 Å)	
Rha A		CDR-H1: Trp H33	
		H3: Gly H95, Gly H96, Ala H97	
Rha B		L1: Tyr L32	
		H3: ALA H97, Gly H99	
Rha C		L1: Tyr L32	
		L3: Thr L91	
		H1: Glu H35	
		H3: Gly H95, Gly H96, Gly H99, Met H100A	
GlcNAc D		L1: His L27D, Tyr L32	
		L3: Thr L91, His L93, Pro L95	
		H2: Glu H50	
Rha A′		L1: His L27D	
		L3: Thr L92, His L93, Val L94	

Table 4: Interactions between BC*D (**2**) and Fab

sugar residue		Fab residue	distance (Å)
		H-bonds (d < 3.4 Å)	
Rha B (3-OH)		CDR-H3: Ala H97 (O)	2.78
	(4-OH)	L1: Tyr L32 (OH)	2.92
Rha C (4-OH)		H3: Gly H96 (O)	3.21
GlcNAc D (2-NH)		L3: Thr L91 (O)	2.63
	(4-OH)	H2: Glu H50 (OE1)	2.84
	(6-OH)	H2: Glu H50 (OE1)	3.38
	(6-OH)	H2: Glu H50 (OE2)	2.83
	(6-OH)	H2: Arg H52 (NH1)	3.37
		H-bonds via H_2O links (d < 3.4 Å)	
GlcNAc D (7-O)		via w3: Arg H52 (NH1, NH2)	
		H-bonds with H_2O (d <3.4 Å)	
Rha B (3-OH)		w1	3.38
	(4-OH)	w2	2.52
GlcNAc D (7-O)		w3	3.06
		van der Waals contacts (d < 4.0 Å)	
Rha B		CDR-L1: Tyr L32	
		H3: Ala H97	
Rha C		L3: Thr L91	
		H1: Trp H33, Glu H35	
		H3: Gly H95, Gly H96, Gly H99	
GlcNAc D		L1: His L27D, Tyr L32	
		L3: Thr L91, Thr L92, His L93, Pro L95	
		H1: Trp H33, Glu H35	
		FR-2: Trp H47	
		CDR-H2: Glu H50, Arg H52, His H58	

group in the hydrophobic pocket as observed in the complex with BC*D. (ii) The C1−C2−N2−C7 torsion angle of the GlcNAc D residue changes by 17° (Figure 4). And (iii) the ϕ and ψ values of the glycosidic bond between the C and D sugar residues in the two complexes differ by 37° and 23°, respectively (Table 5).

Second, the absence of the C2−OH in the BC*D eliminates a polar−nonpolar interaction between the OH group and Tyr L32 present in the complex with ABCDA′ (Figure 4A) and in turn places the resulting C2 methyl group in a favorable hydrophobic interaction with the same aromatic residue (Figure 4B). This hydrophobic interaction is enhanced by the movement of the modified Rha C* closer to the Tyr residue, which is brought about mainly by the changes in the ϕ and ψ torsional angles described above for BC*D relative to those for ABCDA′. The distances of the C2 nonpolar group of the C sugar to the CD2 and CE2 of Tyr L32 in the ABCDA′ complex are 4.9 and 4.8 Å, respectively, whereas those of the C2-methyl group of the C* sugar in the BC*D complex are 4.3 and 4.4 Å, respectively.

Third, due to the absence of C2−OH and the changes in the torsional angles relative to the bound ABCDA′ described above, BC*D makes favorable nonpolar contacts with FR-2 of the heavy chain that are not present in the Fab−ABCDA′ complex. For example, a nonpolar−nonpolar interaction is formed between the C6 methylene group of GlcNAc and the FR2 residue Trp H47 in the Fab−BC*D complex, but it is absent in the complex with ABCDA′ (Tables 3 and 4). A very recent structural study has provided evidence for the dominant role of hydrophobic interaction in binding of oligosaccharides to a protein receptor even when the ligands are able to form significantly more highly specific hydrogen-bonding interactions (*44*). The hydrogen bonds formed in the receptor−carbohydrate interactions, which are mostly neutral−charged type, are considerably more, on a per sugar residue basis, than those described here for the binding of ABCDA′ and BC*D to the Fab.

In addition to the more favorable hydrophobic interactions with BC*D, other features contribute to its tighter binding. The BC*D makes more hydrogen bonds per sugar residue than ABCDA′. Moreover, four of the hydrogen bonds are made with charged residues, whereas only one of these hydrogen bonds, between Glu H50 and C4−OH of the GlcNAc, is present in the Fab−ABCDA′ complex.

The BC*D binds 17-fold more tightly than the natural BCD epitope (*16*). To gain insights into the reason for the deleterious effect of the presence of the C2−OH group, we assume that the natural BCD is bound in a manner very similar to that of the equivalent sugars of ABCDA′. In this case, the hydrophobic interactions that dominate the interaction with the BC*D as described above may not be present in the BCD complex. BCD would also be making two fewer hydrogen bonds than BC*D. More importantly, the network of hydrogen bonds, which involves mainly the GlcNAc D unit, observed in the binding of BC*D, will be absent, including the three charged−neutral hydrogen bonds. Weaker binding of the natural BCD may be also attributed to fewer contacts (∼50, data not shown) with the Fab as compared to that (∼75 contacts) with BC*D. For all the above reasons, the fit of BCD in the binding groove is unlikely to be as good as that of the BC*D analogue.

Induced Fit and Oligosaccharide Conformations. Formation of the complexes is accompanied by changes not only in the structure of the combining site but also in the conformation of the oligosaccharides. Changes in the combining site upon ligand binding are indicated by the minor adjustments of the torsion angles of a few side chains of ligand binding residues, including Trp H33, Glu H35, Glu

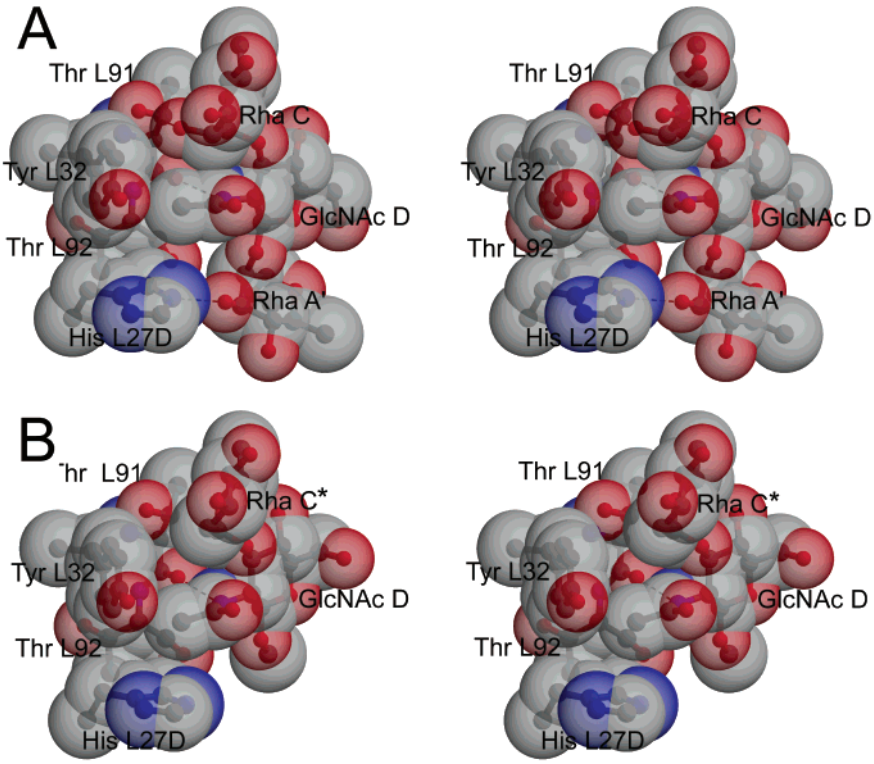

FIGURE 4: Stereoviews (in transparent space-filling models) highlighting only the interactions between the Fab and the CDA′ segment (A) of ABCDA′ and C*D segment (B) of BC*D. The view is centered on the acetamido group of the GlcNAc D residue.

Table 5: Conformations of the Free and Bound Oligosaccharides **1** and **2**

		trisaccharide (BC*D)[a]		pentasaccharide (ABCDA′)[b]	
sugars	glycosidic linkages[c]	$\phi°$	$\psi°$	$\phi°$	$\psi°$
AB	O5−C1−O1−C2′−C3′			−64, −83	−92, −111
BC	O5−C1−O1−C3′−C4′	−63, −71	−129, −136	−82, −93	−116, −155
CD	O5−C1−O1−C3′−C4′	−78, −78	122, 126	−115, −106	145, 51
DA′	O5−C1−O1−C2′−C3′			−90, −104	177, −85

[a] The first value of each torsional angle (ϕ or ψ) is that for BC*D bound to the Fab as determined by X-ray analysis, and the second is the torsional angle of the global minimum energy conformation obtained by force field calculations (GEGOP) (*45*). [b] The first value of each torsional angle (ϕ or ψ) is that for the bound oligosaccharide, and the second is the torsional angle of the average conformation obtained by NMR and molecular dynamics calculations for a heptasaccharide ABCDA′B′C′ (*26*). [c] In the glycosidic linkages, atoms O5, C1, O1 belong to the nonreducing end sugar, and atoms C2′, C3′, C4′ belong to the reducing end sugar. The first four atoms of the glycosidic linkage define the glycosidic angle ϕ and the last four define the glycosidic angle ψ (*3*).

H50, and Met H100A. These changes are partly reflected by the differences in the molecular surfaces of the sugar-binding site groove and surrounding area between the ligand-free and the bound structures, as depicted in Figure 2B−D. However, it is the relative changes in the oligosaccharide conformations that make major differences in the binding between BC*D and ABCDA′.

The conformations of fragments of the *O*-polysaccharide in the free form have been investigated by NMR and molecular modeling studies (*25*, *26*). Table 5 contains a list of these conformations along with those obtained from the structures of the Fab−oligosaccharide complexes. The conformation of BC*D is essentially unchanged upon binding to the protein. In contrast, changes in the conformation, especially of the C−D and D−A′ glycosidic bonds, occur upon binding of ABCDA′. Moreover, the torsion angles of the B−C and C−D glycosidic bonds of the bound ABCDA′ differ considerably from those of the identical bonds in both free and bound trisaccharide (see also Figure 3B,D).

Given the approximations in force field calculations and the flexibility about glycosidic linkages, the conformations are described in general terms by the signs of the torsional angles of the interglycosidic linkages. The conformation of the α-(1−2) linkage of Rha A−Rha B is ϕ -gauche, ψ -gauche (with respect to the heavy atoms, oxygen and carbon), or (−/−), similar to that observed in the average solution conformation of a heptasaccharide ABCDA′B′C′ (Table 5). Similarly, the α-(1−3) Rha B−Rha C linkage has a ϕ -gauche and a ψ -gauche in the X-ray structures of both complexes and the internal Rha-α-(1−3)-Rha linkages in the average conformation of the same heptasaccharide. The α-(1−3) Rha C−GlcNAc D linkage is (−/+), a conformation required by the shape of the site and the interaction primarily of GlcNAc D with the protein. The average conformation in solution shows a ψ angle considerably less than that in the bound crystal structure; rotation around the aglyconic bond is necessary to position GlcNAc D in the site. Finally, the α-(1−2) GlcNAc D−Rha A′ linkage is in the (−/+) conformation, which differs from the (−/−) average conformation observed in solution. Again, rotation around the aglyconic bond is necessary for the A′ ring to fit in the site and form a hydrogen bond to His L27D (Figure 3C). This

conformation is similar to the calculated solution global minimum (*26*).

In the corresponding Fab−BC*D complex structure, the positions of the three sugar residues in the binding groove generally follow those of the three middle rings (BCD) of ABCDA′ (Figure 2A). However, deoxygenation at C2 of Rha C* causes both ϕ and ψ glycosidic angles of the Rha B−Rha C* and the Rha C*−GlcNAc D linkages to change relative to the angles of the bound ABCDA′ (Table 5). These concerted changes have three major favorable effects in BC*D binding. First, they allow the formation of a hydrogen bond between the 4-OH group of Rha C* and the carbonyl oxygen of H96. Second, they enable the 7-oxygen of the *N*-acetamido group of the D sugar to link via a water molecule with Arg H52. Third and more importantly, as described above, they promote better hydrophobic interactions of the methyl groups at the C8 position of the D sugar and the C2 position of the 2-deoxy C* sugar. As also described above, a change in the torsional angles of the exocyclic C6−OH of BC*D, relative to ABCDA′, shows another dramatic conformational change favorable to ligand binding.

A Model of Binding of Internal Repeating Units of the O-Antigen Polysaccharide. With the Fab−ABCDA′ structure providing a rational basis, a model of the bound *S. flexneri O*-antigen polysaccharide was built (see Methods). In the modeling, we took into consideration the prior prediction that the *O*-antigen is a left-handed helix composed of eight linear sugars (ABCDA′B′C′D′) or two tetrasaccharide repeating units related by a 2-fold screw axis parallel to the helix axis (*25*). A linear helical chain of three repeating ABCD tetrasaccharide units (A″B″C″D″ABCDA′B′C′D′) was sufficient to reveal a plausible model of a bound *O*-polysaccharide antigen (Figure 2E). The model demonstrates that the B″C″D″ABCDA′ sequence of the polysaccharide could fit easily in the binding groove without steric clashes (Figure 2E), but only six sugar residues (B″ and ABCDA′) are contacting protein residues. Since the B″ sugar makes only one of the total 82 contacts between the modeled hexasaccharide and Fab, the major determinant for the helical *O*-antigen recognition is almost entirely associated with the ABCDA′ segment.

O-Polysaccharide-specific antibodies produced in mice against *S. flexneri* are specific for either the nonreducing end or the internal repeating sugars (*46*). Our crystallographic data do not provide a clear resolution between these two choices, but the following observations strongly indicate that the SYA/J6 mAb is designed to recognize internal linear repeating epitopes. First, the nonreducing terminal sugar (Rha A) of the bound pentasaccharide is partially exposed. The C2−OH of the pentasaccharide, which is involved in a glycosidic bond with the Rha D″ from the preceding internal repeating unit of the *O*-polysaccharide (Figure 2E), is solvent accessible and makes no hydrogen bond with the Fab in the bound structure. Second, extension from Rha A of the bound pentasaccharide, as was done in the modeling of a bound left-handed helical polysaccharide antigen, is straightforward and free from steric clashes (Figure 2E). And, third, the binding site is definitely a groove, the type meant for binding internal oligosaccharide sequences by a mAb (*47*). This type of binding site is clearly different than the pocketlike or deep cavity site required for binding and burying a terminal sugar residue of a polysaccharide antigen, as clearly revealed in the crystal structures of the BR96 and S-20-24 Fabs, which are known to bind terminal sugars (*4*, *5*). The structure of Se 155−4 with bound oligosaccharide portrays another example of a groovelike site for binding an internal oligosaccharide epitope (*3*), although the site differs from that of the SYA/J6 mAb. A large portion of the groove in SYA/J6 is located deeper (Figure 2) than that in Se 155−4. In fact, with the exception of a cavity for binding the internal Abe sugar residue, the groove in Se 155−4 is for the most part on the surface. Moreover, the groove in SYA/J6 runs parallel to the interface of the V_L and V_H domains, whereas the surface groove in Se 155−4 is roughly perpendicular to these domains. These differences suggest that the binding site in SYA/J6 is thus far the best example of a groovelike site for binding an internal oligosaccharide epitope.

Table 6: Thermodynamic Parameters for Oligosaccharide Ligands **1**−**12** Bound to *S. flexneri* Antibody SYA/J6 at 25 °C

oligosaccharide	K_A[a]	ΔG[b]	ΔH[b]	$-T\Delta S$[b]
1	2.5×10^5	−7.4	−1.5	−5.9
2	1.7×10^6	−8.4	−10.1	+1.6
3	9.5×10^4	−6.8	−4.3	−2.5
4	2.0×10^5	−7.2	−3.4	−3.8
5[c]	3.8×10^4	−6.3[d]	nd	nd
6	3.3×10^4	−6.2	−2.9	−3.3
7[c]	4.7×10^4	−6.4[d]	nd	nd
8[c]	inactive			
9[c]	2.9×10^4	−6.1[d]	nd	nd
10	3.2×10^6	−8.9	−6.6	−2.3
11	2.8×10^4	−6.1	−1.8	−4.2
12	9.1×10^4	−6.8	−2.5	−4.3

[a] Binding constants expressed in M^{-1}; the standard deviation for duplicate measurements of K_A was never greater than ±2%. [b] Thermodynamic parameters ΔH, ΔG, and $T\Delta S$ expressed in kcal mol^{-1}. The standard deviation on ΔH for duplicate measurements did not exceed ±5%. [c] Data from ref 16. [d] Estimated from solid-phase binding assays.

Calorimetry. The thermodynamic data deal with pentasaccharide **1**, tetrasaccharide **4**, trisaccharide BCD **3**, its monodeoxy analogues **2** and **5**−**9**, the monochlorodeoxy trisaccharide **10**, and the *N*-acyl analogues **11** and **12** (Figure 1 and Table 6). These data shed light on the strength of certain hydrogen bonds, as well as highlighting the importance of van der Waals and nonpolar interactions.

Certain generalizations have emerged from mapping the energetics of carbohydrate−protein interactions (*16*, *48*−*52*). These may be summarized: replacement of a hydroxyl group by hydrogen (monodeoxygenation) or halides changes the binding energy $\Delta(\Delta G)$ by 1−1.5 kcal mol^{-1} and is most often associated with hydrogen bonds between charged donor/acceptor pairs; a $\Delta(\Delta G)$ of 0.5−1.0 kcal mol^{-1} suggests the possibility of neutral donor/acceptor hydrogen bonds, and $\Delta(\Delta G)$ ~0.25−0.5 kcal mol^{-1} are assigned to weaker polar contacts or solvent-exposed hydrogen bonds (*49*).

The variation of the thermodynamic parameters with epitope size exhibits an interesting trend. Pentasaccharide **1** binds more tightly than the tetrasaccharide **4**, which in turn binds more tightly than BCD **3**. In this series the favorable enthalpic contribution to binding increases in the series **1** < **4** < **3** ≪ **2**, while the entropy change becomes less favorable across the series. Relative to **3**, the much more favorable and dominant enthalpic term associated with the binding of

2 is consistent with the larger number of oligosaccharide−protein contacts and the accompanying loss of entropy associated with immobilizing more bonds. In sharp contrast to binding of **3**, the binding energy of pentasaccharide **1** is a predominantly entropy-driven process. Since the bound form of ABCDA′ adopts a conformation about two of the four glycosidic linkages that departs from the average solution conformation, this may represent part of the enthalpic penalty. Enthalpic losses on binding **1** may arise from unfavorable van der Waals contacts between saccharide ligand and protein as the Rha A′ residue protrudes from the binding site, as is evident from the Fab−**1** complex. Entropy gains can occur when the additional rhamnose residue A′ displaces water molecules (*53*). A similar situation pertains to the Rha A residue at the other end of the binding cleft, since a comparison of the binding data for tetrasaccharide **4** with BCD **3** shows a less favorable enthalpy of binding with a concomitant increase in entropy.

Free energy changes that accompany functional group modifications (e.g. trisaccharide congeners **5**−**12**) are compared with the native BCD **3**. Structural correlations of these free energy changes are made with the Fab−ABCDA′ complex, since it is only within this complex that the binding of the trisaccharide BCD **3** can be observed as described above.

Monodeoxygenation at C4 of GlcNAc D yields an inactive inhibitor and is therefore consistent with a strong hydrogen bond to a charged amino acid side chain (Glu H50). Since the threshold for usable microcalorimetry measurements corresponds to $\Delta G = 4.0-5.0$ kcal mol^{-1}, a loss of binding energy of at least 2−2.5 kcal mol^{-1} must accompany this deoxygenation, since BCD **3** has a binding energy of −6.8 kcal mol^{-1}. Although GlcNAc C6−OH is involved as an acceptor in the network of cooperative hydrogen bonds with Glu H50 for the Fab−**2** complex, the Fab−**1** does not show this H-bond network. Nevertheless, deoxygenation at this position (compound **9**) leads to a 0.7 kcal mol^{-1} loss of binding. The origins of this free energy change cannot be related to any discernible structural features. The acetamido group of the GlcNAc residue is essential to binding, since its replacement by OH leads to an inactive compound (*16*). The crystal structures indicate a hydrogen bond between the amide NH and Thr L91 O and favorable nonpolar contacts of the acetamido methyl group in the hydrophobic pocket formed by Tyr L32, His L27D, and Thr L91. The combined importance of the latter is indicated by the decreased binding energy when $NHCOCH_3$ (**3**) is replaced by the more polar $NHCOCF_3$ (**11**) ($\Delta\Delta G = +0.7$ kcal mol^{-1}) or the sterically more demanding propionamide group (**12**).

The hydrogen bonds Ala H97 to Rha B O3 and Tyr L32 to Rha B O4 observed in the Fab−**1** and Fab−**2** complexes are relatively weak hydrogen bonds as judged by the loss of 0.5−0.6 kcal mol^{-1} in free energy of binding for the 3-deoxy and 4-deoxy compounds **5** and **6**.

The Rha C residue is completely buried in the binding site and is inaccessible to a water probe. A low-energy hydrogen bond (0.4 kcal mol^{-1} cf **3** vs **7**) from Rha C4−OH to Gly H96 O is present in the complex with BC*D **2** but not in the ABCDA′ complex. Like the deoxygenation at GlcNAc C6, there is no apparent detail with which to correlate this free energy change. Monodeoxy- and monochlorodeoxytrisaccharides **2** and **10** exhibit significantly enhanced binding relative to **3**. Monodeoxygenation results in better van der Waals contacts ($\Delta\Delta H = -5.8$ kcal mol^{-1}) between the Fab and BC*D which, as described above, are associated with the removal of the C2−OH group. The less favorable entropy change ($\Delta(T\Delta S) = +4.1$ kcal mol^{-1}) is consistent with the greater restriction of motion in the complex. Substitution of Rha C2−OH by chlorine results in enthalpic gain ($\Delta\Delta H = -2.3$ kcal mol^{-1}) and negligible entropy change. We propose that compound **10**, like **3**, cannot penetrate into the site as well as **2**, because Cl is of similar size to OH in **3**. However, a compensating Cl to Tyr L32 stabilizing interaction may account for the enthalpy change.

CONCLUSIONS

The principal conclusions that can be drawn from this study are as follows. (i) The combining site of the Fab of mAb SYA/J6 is a long groove that is able to accommodate and contact a pentasaccharide segment (Rha A−Rha B−Rha C−GlcNAc D−Rha A′), which is one residue (A′) longer than the biological repeating unit of the LPS. (ii) For both ABCDA′ and BC*D, the disaccharide element CD or C*D makes the dominant contribution to the recognition by the antibody. While residue C or C* is completely buried in a deep pocket near the center of the groove-shaped binding site, the partially solvent-exposed residue D is involved in the largest number of polar contacts without which recognition is lost. (iii) The penetration of residue C into the deep pocket as well as the positioning of the BCD segment of ABCDA′ is accomplished by conformational changes of the ϕ,ψ angles in glycosidic linkages relative to the unbound conformation. (iv) BC*D retains essentially its conformation after binding to the Fab. (v) The structure analysis uncovered at least three reasons for tighter binding of the modified trisaccharide than the pentasaccharide. The trisaccharide is more buried and fits more snugly in the groove than the pentasaccharide. It makes as many contacts with the Fab as the pentasaccharide. It is engaged in more favorable hydrophobic interactions with the Fab than the pentasaccharide. (vi) SYA/J6 mAb is likely to recognize internal repeating epitopes rather than the nonreducing end of the *O*-polysaccharide antigen. (vii) Thermodynamic data for the congeners **4**−**12** show that the native tri- to pentasaccharides have free energies of binding in the range of 6.8−7.4 kcal mol^{-1}. With the exception of C4−OH of the GlcNAc residue, the hydrogen bonds to individual hydroxyl groups are relatively weak and none provide more than ∼0.7 kcal mol^{-1}. Hydrophobic interactions make significant contributions to binding, and as the native epitope becomes larger across the series tri-, tetra-, pentasaccharide **3**, **4** and **1**, entropy contributions to the free energy become dominant.

ACKNOWLEDGMENT

We thank Professor N. Sakabe and the staff at the Photon Factory for assistance.

REFERENCES

1. Lindberg, A. A. (1999) *C. R. Acad. Sci. III 322*, 925−932.
2. Wolchok, J. D., and Livingston, P. O. (2001) *Lancet Oncol. 2*, 205−211.
3. Cygler, M., Rose, D. R., and Bundle, D. R. (1991) *Science 253*, 442−445.

4. Villeneuve, S., Souchon, H., Riottot, M. M., Mazie, J. C., Lei, P., Glaudemans, C. P., Kovac, P., Fournier, J. M., and Alzari, P. M. (2000) *Proc. Natl. Acad. Sci. U.S.A. 97*, 8433−8438.
5. Jeffrey, P. D., Bajorath, J., Chang, C. Y., Yelton, D., Hellstrom, I., Hellstrom, K. E., and Sheriff, S. (1995) *Nat. Struct. Biol. 2*, 466−471.
6. Rose, D. R., Przybylska, M., To, R. J., Kayden, C. S., Oomen, R. P., Vorberg, E., Young, N. M., and Bundle, D. R. (1993) *Protein Sci. 2*, 1106−1113.
7. Evans, S. V., Rose, D. R., To, R., Young, N. M., and Bundle, D. R. (1994) *J. Mol. Biol. 241*, 691−705.
8. Patenaude, S. I., Vijay, S. M., Yang, Q. L., Jennings, H. J., and Evans, S. V. (1998) *Acta Crystallogr. D 54*, 1005−1007.
9. Evans, S. V., Sigurskjold, B. W., Jennings, H. J., Brisson, J. R., To, R., Tse, W. C., Altman, E., Frosch, M., Weisgerber, C., Kratzin, H. D., et al. (1995) *Biochemistry 34*, 6737−6744.
10. Paoletti, L. C., Kasper, D. L., Michon, F., DiFabio, J., Jennings, H. J., Tosteson, T. D., and Wessels, M. R. (1992) *J. Clin. Invest. 89*, 203−209.
11. Inouye, M. (1979) in *Bacterial Outer Membrane* (Inouye, M., Ed.) pp 1−12, Wiley, New York.
12. Brahmbhatt, H. N., Lindberg, A. A., and Timmis, K. N. (1992) *Curr. Top. Microbiol. Immunol. 180*, 45−64.
13. Pozsgay, V., Chu, C., Pannell, L., Wolfe, J., Robbins, J. B., and Schneerson, R. (1999) *Proc. Natl. Acad. Sci. U.S.A. 96*, 5194−5197.
14. Svenson, S. B., and Lindberg, A. A. (1981) *Infect. Immun. 32*, 490−496.
15. Vyas, M. N., Vyas, N. K., Meikle, P. J., Sinnott, B., Pinto, B. M., Bundle, D. R., and Quiocho, F. A. (1993) *J. Mol. Biol. 231*, 133−136.
16. Bundle, D. R. (1999) in *Bioorganic Chemistry (Carbohydrates)* (Hecht, S. M., Ed.) pp 370−440, Oxford University Press, Oxford.
17. Bundle, D. R. (1989) *Pure Appl. Chem. 61*, 1171−1180.
18. Brady, R. L., Edwards, D. J., Hubbard, R. E., Jiang, J. S., Lange, G., Roberts, S. M., Todd, R. J., Adair, J. R., Emtage, J. S., King, D. J., et al. (1992) *J. Mol. Biol. 227*, 253−264.
19. Higashi, T. (1989) *J. Appl. Crystallogr. 22*, 9−18.
20. Satow, Y., Cohen, G. H., Padlan, E. A., and Davies, D. R. (1986) *J. Mol. Biol. 190*, 593−604.
21. Brünger, A. T., Adams, P. D., Clore, G. M., DeLano, W. L., Gros, P., Grosse-Kunstleve, R. W., Jiang, J. S., Kuszewski, J., Nilges, M., Pannu, N. S., Read, R. J., Rice, L. M., Simonson, T., and Warren, G. L. (1998) *Acta Crystallogr. D 54*, 905−921.
22. Sack, J. S. (1988) *J. Mol. Graphics 6*, 224−225.
23. Laskowski, R., MacArthur, M., Moss, D., and Thornton, J. (1993) *J. Appl. Crystallogr. 26*, 283−291.
24. Luzzati, V. (1952) *Acta Crystallogr. 5*, 802−810.
25. Bock, K., Josephson, S., and Bundle, D. R. (1982) *J. Chem. Soc., Perkin Trans. 2*, 59−70.
26. Kreis, U., Varma, V., and Pinto, B. (1997) *J. Mol. Struct. (THEOCHEM) 395*−*396*, 389−409.
27. Gill, S. C., and von Hippel, P. H. (1989) *Anal. Biochem. 182*, 319−326.
28. Chervenak, M. C., and Toone, E. J. (1994) *J. Am. Chem. Soc. 116*, 10533−10539.
29. Wiseman, T., Williston, S., Brandts, J. F., and Lin, L. N. (1989) *Anal. Biochem. 179*, 131−137.
30. Bundle, D. R., Alibés, R., Nilar, S., Otter, A., Warwas, M., and Zhang, P. (1998) *J. Am. Chem. Soc. 120*, 5317−5318.
31. Padlan, E. A. (1994) *Mol. Immunol. 31*, 169−217.
32. Al-Lazikani, B., Lesk, A. M., and Chothia, C. (1997) *J. Mol. Biol. 273*, 927−948.
33. Chothia, C., Lesk, A. M., Tramontano, A., Levitt, M., Smith-Gill, S. J., Air, G., Sheriff, S., Padlan, E. A., Davies, D., Tulip, W. R., et al. (1989) *Nature 342*, 877−883.
34. Martin, A. C., and Thornton, J. M. (1996) *J. Mol. Biol 263*, 800−815.
35. Morea, V., Tramontano, A., Rustici, M., Chothia, C., and Lesk, A. M. (1998) *J. Mol. Biol. 275*, 269−294.
36. Zhou, G. W., Guo, J., Huang, W., Fletterick, R. J., and Scanlan, T. S. (1994) *Science 265*, 1059−1064.
37. Guarné, A., Bravo, J., Calvo, J., Lozano, F., Vives, J., and Fita, I. (1996) *Protein Sci. 5*, 167−169.
38. Derrick, J. P., Maiden, M. C., and Feavers, I. M. (1999) *J. Mol. Biol. 293*, 81−91.
39. Ferrin, T., Huang, C., Jarvis, L., and Langridge, R. (1988) *J. Mol. Graphics 6*, 13−27.
40. Nicholls, A., Sharp, K. A., and Honig, B. (1991) *Proteins: Struct., Funct., Genet. 11*, 281−296.
41. Lee, B., and Richards, F. M. (1971) *J. Mol. Biol. 55*, 379−400.
42. Dougherty, D. A. (1996) *Science 271*, 163−168.
43. Kraulis, P. (1991) *J. Appl. Crystallogr. 24*, 946−950.
44. Duan, X., and Quiocho, F. A. (2002) *Biochemistry 41*, 706−712.
45. Stuike-Prill, R., and Meyer, B. (1990) *Eur. J. Biochem. 194*, 903−919.
46. Carlin, N. I., Bundle, D. R., and Lindberg, A. A. (1987) *J. Immunol. 138*, 4419−4427.
47. Cisar, J., Kabat, E. A., Dorner, M. M., and Liao, J. (1975) *J. Exp. Med. 142*, 435−459.
48. Lemieux, R. U. (1996) *Acc. Chem. Res. 29*, 373−380.
49. Nikrad, P. V., Beierbeck, H., and Lemieux, R. U. (1992) *Can. J. Chem. 70*, 241−353.
50. Vermersch, P. S., Tesmer, J. J., and Quiocho, F. A. (1992) *J. Mol. Biol. 226*, 923−929.
51. Glaudemans, C. P. J. (1991) *Chem. Rev. 91*, 25−33.
52. Street, I. P., Armstrong, C. R., and Withers, S. G. (1986) *Biochemistry 25*, 6021−6027.
53. Dunitz, J. D. (1995) *Chem. Biol. 2*, 709−712.

BI0261387